JACS
JOURNAL OF THE AMERICAN CHEMICAL SOCIETY

Article

Monoamine Oxidase A Inhibitor – Near-Infrared Dye Conjugate Reduces Prostate Tumor Growth

Jason Boyang Wu, Tzu-Ping Lin, John David Gallagher, Swati Kushal, Leland W. K. Chung, Haiyen Zhau, Bogdan Z Olenyuk, and Jean C. Shih

J. Am. Chem. Soc., **Just Accepted Manuscript** • DOI: 10.1021/ja512613j • Publication Date (Web): 13 Jan 2015

Just Accepted

Journal of the American Chemical Society is published by the American Chemical Society. 1155 Sixteenth Street N.W., Washington, DC 20036

Monoamine Oxidase A Inhibitor – Near-Infrared Dye Conjugate Reduces Prostate Tumor Growth

Jason Boyang Wu,[†] Tzu-Ping Lin,[§,‡] John D. Gallagher,[‡] Swati Kushal,[‡]
Leland W.K. Chung,[†] Haiyen E. Zhau,[,†] Bogdan Z. Olenyuk,[*,‡,∥] and Jean C. Shih[*,‡,⊥]*

Addresses:

[†]Uro-Oncology Research Program, Department of Medicine, Samuel Oschin Comprehensive Cancer Institute, Cedars-Sinai Medical Center, Los Angeles, CA 90048, U.S.A.

[‡]Department of Pharmacology and Pharmaceutical Sciences, School of Pharmacy, University of Southern California, Los Angeles, CA 90089, U.S.A.

[⊥]Department of Cell and Neurobiology, Keck School of Medicine, University of Southern California, 1975 Zonal Ave., Los Angeles, CA 90033, U.S.A.

[∥]USC Norris Comprehensive Cancer Center, 1441 Eastlake Avenue, Los Angeles, CA 90033, U.S.A.

[§]Current addresses: Department of Urology, Taipei Veterans General Hospital, Taipei, Taiwan 11217, R.O.C., and Department of Urology, School of Medicine, and Shu-Tien Urological Research Center, National Yang-Ming University, Taipei, Taiwan 11217, R.O.C.

*Corresponding authors:

Jean C. Shih, Department of Pharmacology and Pharmaceutical Sciences, 1985 Zonal Ave., PSC 518, Los Angeles, CA 90089, U.S.A. Tel.: +1-323-442-1441; E-mail: jcshih@usc.edu

Bogdan Z. Olenyuk, Department of Pharmacology and Pharmaceutical Sciences, 1985 Zonal Ave., PSC B15C, Los Angeles, CA 90089, U.S.A. Tel.: +1-323-442-1390; E-mail: bogdan@usc.edu.

Haiyen E. Zhau, Uro-Oncology Research Program, Department of Medicine, Samuel Oschin Comprehensive Cancer Institute, Cedars-Sinai Medical Center, Los Angeles, CA 90048, U.S.A. Tel.: +1-310-423-5992; E-mail: haiyen.zhau@cshs.org

Abstract

Development of anticancer agents with high tumor-targeting specificity and efficacy are critical goals of modern multidisciplinary cancer research. Monoamine oxidase A (MAOA), a mitochondria-bound enzyme, degrades monoamine neurotransmitters and dietary monoamines. Recent evidence suggests correlation between increased MAOA expression and prostate cancer (PCa) progression with poor outcomes for patients. MAOA induces epithelial-mesenchymal transition (EMT) and augments hypoxic effects by producing excess reactive oxygen species. Thus, development of MAOA inhibitors which selectively target tumors becomes an important goal in cancer pharmacology. Here we describe the design, synthesis, *in vitro* and *in vivo* evaluation of **NMI**, a conjugate that combines a near-infrared dye for tumor targeting with the moiety derived from MAOA inhibitor clorgyline. **NMI** inhibits MAOA with low micromolar IC_{50}, suppresses PCa cell proliferation, colony formation and reduces migration and invasion. In mouse PCa xenografts, **NMI** targets tumor with no detectable accumulation in normal tissues, providing effective reduction of the tumor burden. Analysis of tumor specimens shows reduction in Ki-67^+ and $CD31^+$ cells, suggesting decrease of cell proliferation and angiogenesis, and increase in $M30^+$ cells, indicating increased apoptosis. Gene expression profiles of tumors treated with **NMI** demonstrate reduced expression of oncogenes *FOS*, *JUN*, *NFKB*, *MYC*, and cell cycle regulators *CCND1*, *CCNE1*, *CDK4*/*6*, and increase in the levels of tumor suppressor gene *TP53*, cell cycle inhibitors *CDKN1A* and *CDKN2A* and MAOA-downstream genes that promote EMT, tumor hypoxia, cancer cell migration and invasion. These data suggest that **NMI** exerts its effect through tumor-targeted delivery of MAOA-inactivating group, making **NMI** a valuable anti-tumor agent.

Introduction

The search for new targets and development of anticancer agents with high tumor targeting specificity and efficacy are critical goals underpinning the urgent, unmet need for more effective, mechanism-based cancer therapies. Monoamine oxidase A (MAOA) is a mitochondria-bound enzyme which catalyzes the degradation of monoamine neurotransmitters and dietary amines by oxidative deamination.[1,2] This process is accompanied by production of hydrogen peroxide (H_2O_2), a major source of reactive oxygen species (ROS), which can predispose cancer cells to DNA damage and can be a main cause of tumor initiation and progression.[3,4] Recent studies performed by us[5] and others[6] have shown that increased MAOA levels are associated with prostate cancer (PCa) progression and poor prognosis for patients,[7] and pharmacological inhibition of MAOA reduces the growth of PCa cells *in vitro* and tumor xenografts *in vivo*.[5,8] PCa is the second most common cause of death from cancer in American men of all ages.[9] Despite its widespread occurrence, current treatments that include hormonal therapy,[10] radiation therapy[11] and surgery[12] are beneficial only for patients in the early stages of the disease and result in undesired side effects. These treatments have limited effectiveness for patients with advanced stages of castration-resistant and metastatic PCa. The urgent, unmet need for novel, effective mechanism-based therapies with reduced side effects facilitated search for novel targets in PCa and their pharmacological inhibitors.

We found that overexpression of MAOA in human PCa cell lines results in a loss of cell polarity, cell-cell adhesion, and gain of migratory and invasive properties, indicating that MAOA induces epithelial-mesenchymal transition (EMT).[5] Moreover, MAOA-dependent activation of oncogenic pathways was consistently detected in high-grade PCa specimens, and knockdown of

MAOA reduced or even eliminated prostate tumor growth and metastasis in a variety of PCa xenograft mouse models. By conducting site-directed mutagenesis we found that MAOA catalytic activity is the major reason for enhancing growth and metastasis of PCa.[5] MAOA produces hydrogen peroxide as a by-product of oxidative deamination reactions taking place in the outer membrane of mitochondria. Hydrogen peroxide and products of its conversion as other forms of ROS stabilize hypoxia-inducible factor 1 α (HIF1α).[13-15] HIF1α increases tumor angiogenesis, survival responses as well as invasion and metastasis through the overexpression of hypoxia-inducible genes.[16,17] These results are fully consistent with the clinical data, where elevated MAOA expression in PCa tissues is correlated with poor prognosis for PCa patients.[7]

In keeping with these observations, we investigated MAOA as a potential novel pharmacological target for the treatment of human PCa. MAOA inhibitors, many of which are currently on the market as antidepressants,[1] target central nervous system and other peripheral tissues where MAOA is present. This reduces effective systemic concentration of MAOA inhibitors limiting their delivery into the tumor where they could be most effective. To circumvent these problems we designed a novel tumor-targeted MAOA inhibitor that would preferentially accumulate in the cancerous lesions. This inhibitor contains tumor-targeting near-infrared (NIR) dye and a moiety of MAOA inhibitor. We reasoned that including an NIR imaging functionality could be useful for measuring uptake and cellular localization of the conjugate and possibly, for future image-guided diagnosis and drug delivery. We chose small molecule clorgyline as a MAOA-targeting functionality because of the high affinity and selectivity of this compound towards MAOA. The presence of high-resolution crystal structure of clorgyline-MAOA complex[18] facilitated our design. For tumor-targeting and NIR-imaging we chose a recently developed class of non-toxic,

fluorescent heptamethine carbocyanine dyes with NIR emission maxima.[19-21] The high selectivity in targeting of these dyes to tumors, mediated by tumor hypoxia and organic anion-transporting polypeptides (OATPs),[22] has been demonstrated for many types of cancers, including human PCa.[23] Here we report the first study on PCa targeting and inhibition of xenograft growth in mice with designed dual-function NIR dye – MAOA inhibitor conjugate (Figure 1A), abbreviated as **NMI**.

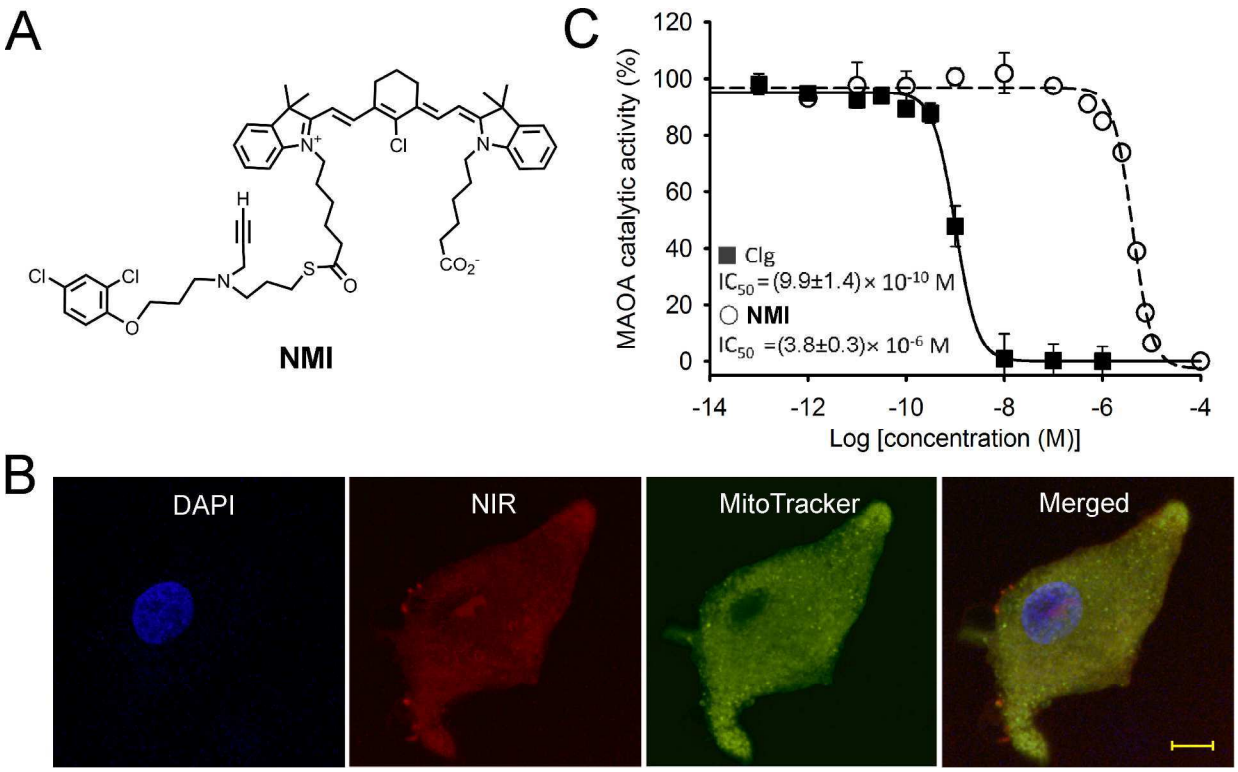

Figure 1. Structure and *in vitro* characterization of **NMI**.
(A) Chemical structure of **NMI**. (B) Confocal images of a single LNCaP cell incubated with NMI. DAPI and MitoTracker agent were used to stain the nucleus and mitochondria of cells, respectively. Scale bar: 10 μm. (C) Inhibition of MAOA activity was determined in C4-2B cells (see Experimental Section). Clorgyline (Clg) or **NMI** were pre-incubated at 37°C for 20 min at indicated doses and IC_{50} were determined. The assay was performed in triplicate.

Results

Design and synthesis of NMI.

NMI has been synthesized in a sequence of steps outlined in Scheme 1. The synthesis started with commercially available 3-bromopropylamine hydrobromide **1**. This compound was converted into *t*-butyl (3-bromopropyl)carbamate **2**, which was used in the subsequent step to alkylate the commercially available 2,4-dichlorophenol, giving an intermediate **4**. Deprotonation of the amide in **4** was carried out with sodium hydride, followed by alkylation with propargyl bromide **5**, producing Boc-protected alkyne **6**. The protecting group was removed under acidic conditions using TFA in dichloromethane. The product **7** was alkylated with 1-bromo-3-thioacetylpropane **8**, resulting in the formation of compound **9**. Removal of the acetyl protective group in **9** was carried out in methanolic HCl, affording an intermediate **10**. This intermediate

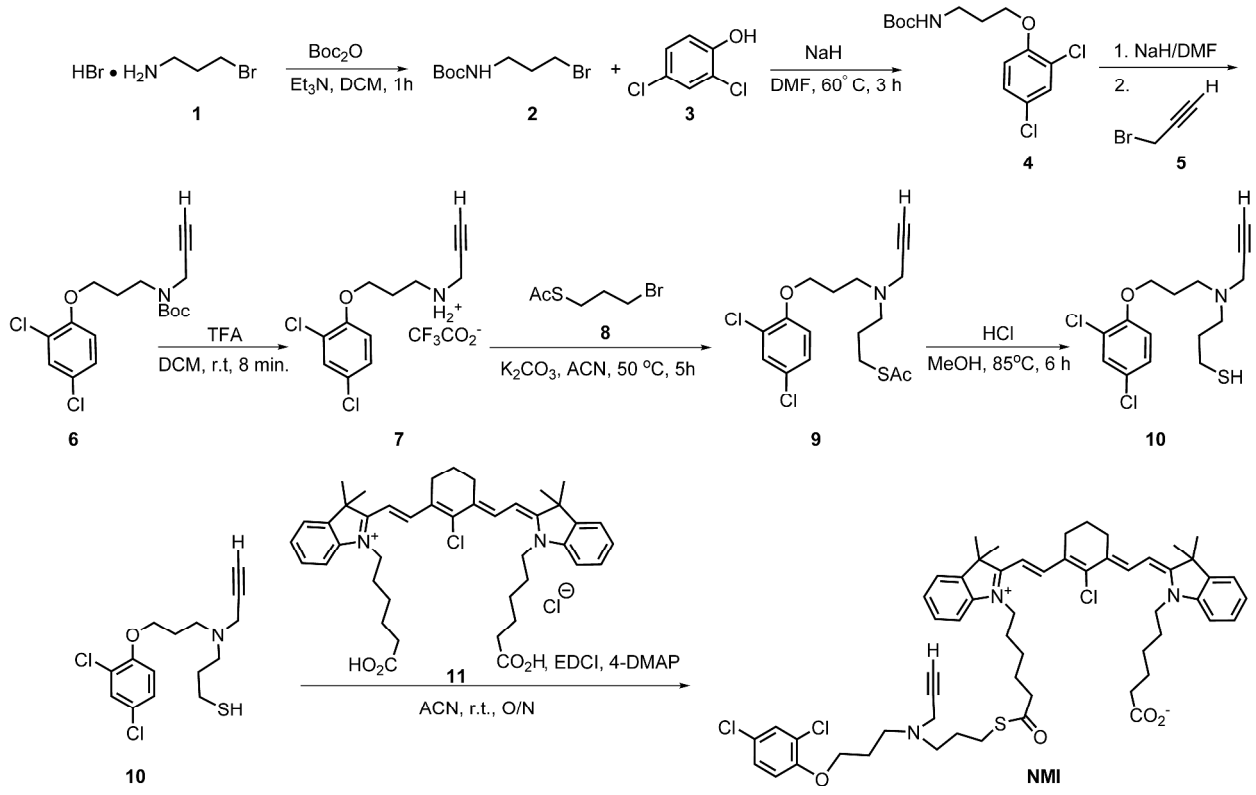

Scheme 1. Synthesis of NIR dye – MAOA inhibitor conjugate **NMI.**

was then coupled to MHI-148 dye **11** using EDCI and 4-DMAP to give the product **NMI** in good yield (Scheme 1). The compound was purified on preparative TLC and its identity and purity were confirmed by NMR and mass spectrometry.

NMI localizes in PCa cells and inhibits MAOA.

Recent reports suggested that the NIR hepatamethine carbocyanine dyes IR-783 and MHI-148 can be retained in cancer cells but not normal cells, in tumor xenografts and in spontaneous tumors in transgenic mice.[23] The two dyes have strong emission maxima at 820-860 nm upon excitation at 750-780 nm, which can be easily detected by NIR imaging. MAOA inhibitor-monomethine carbocyanine conjugates have similar fluorescence properties as the NIR dye MHI-148 itself. Therefore, laser-scanning confocal microscope equipped with the appropriate laser and filters for NIR imaging was used to examine the cellular uptake of **NMI** in human PCa LNCaP cells which have high MAOA levels. Images of a single cell treated with **NMI** are shown in Figure 1B (*vide supra*). This compound rapidly accumulated in LNCaP cells and localized in the mitochondria, as determined by the co-staining with the mitochondria-specific dye MitoTracker Green. In order to test the inhibitory activity of **NMI**, an MAOA activity assay was carried out in LNCaP-derived C4-2B cells using radiolabeled MAOA-specific substrate serotonin. The results indicate that **NMI** inhibits MAOA activity with the mean IC_{50} of (3.8 $\pm 0.3) \times 10^{-6}$ M (Figure 1C).

NMI reduces colony formation, migration and invasion of PCa cells.

PCa LNCaP, C4-2B and MAOA-overexpressing PC-3 cells[5] were used for cell viability (Figure 2A) and cell proliferation assays (Figure 2B). Treatment with clorgyline produced dose response

curves with 50% inhibitory concentrations (IC_{50}) of 80.7 ± 8.8 μM in LNCaP, 113.5 ± 8.0 μM in C4-2B, and 129.3 ± 9.6 μM in MAOA-overexpressing PC-3 cells. By comparison, treatment with **NMI** produced curves with IC_{50} of 5.1 ± 0.1 μM in LNCaP, 5.6 ± 0.1 μM in C4-2B, and 6.1 ± 0.2 μM in MAOA-overexpressing PC-3 cells, indicating 12-20 times higher efficacy for **NMI** in inhibiting PCa cells growth as compared to clorgyline (Figure 2A).

Most PCa cell lines, including LNCaP, C4-2B and MAOA-overexpressing PC-3, possess low, undetectable levels of monoamine oxidase B (MAOB), the second known MAO isoform.[24] However, given the important role MAOB plays in normal physiology of the central nervous system and peripheral tissues,[2] we first decided to ascertain that MAOA is selectively inhibited with minimal interference to MAOB. Given that clorgyline is selective for MAOA and produces dose-sensitive inhibition,[2] in our preliminary cell-based assays we used a range of clorgyline concentrations (10 nM – 10 μM) that are inhibitory for MAOA but below the IC_{50} for MAOB inhibition.[25] We determined 1 μM concentration as the lowest required for clorgyline showing efficacy in suppressing cell proliferation. This concentration was also consistent with the data from other reported study.[24] Thus, we chose 1 μM as the concentration at which the efficacies of both clorgyline and **NMI** could be assessed and compared in the subsequent *in vitro* studies.

In cell number counting assays we observed that both clorgyline and **NMI** reduced the number of proliferating cells after 12 days. **NMI** also showed higher efficacy as compared to clorgyline (Figure 2B). Colony formation assays were performed in LNCaP cells treated with clorgyline or

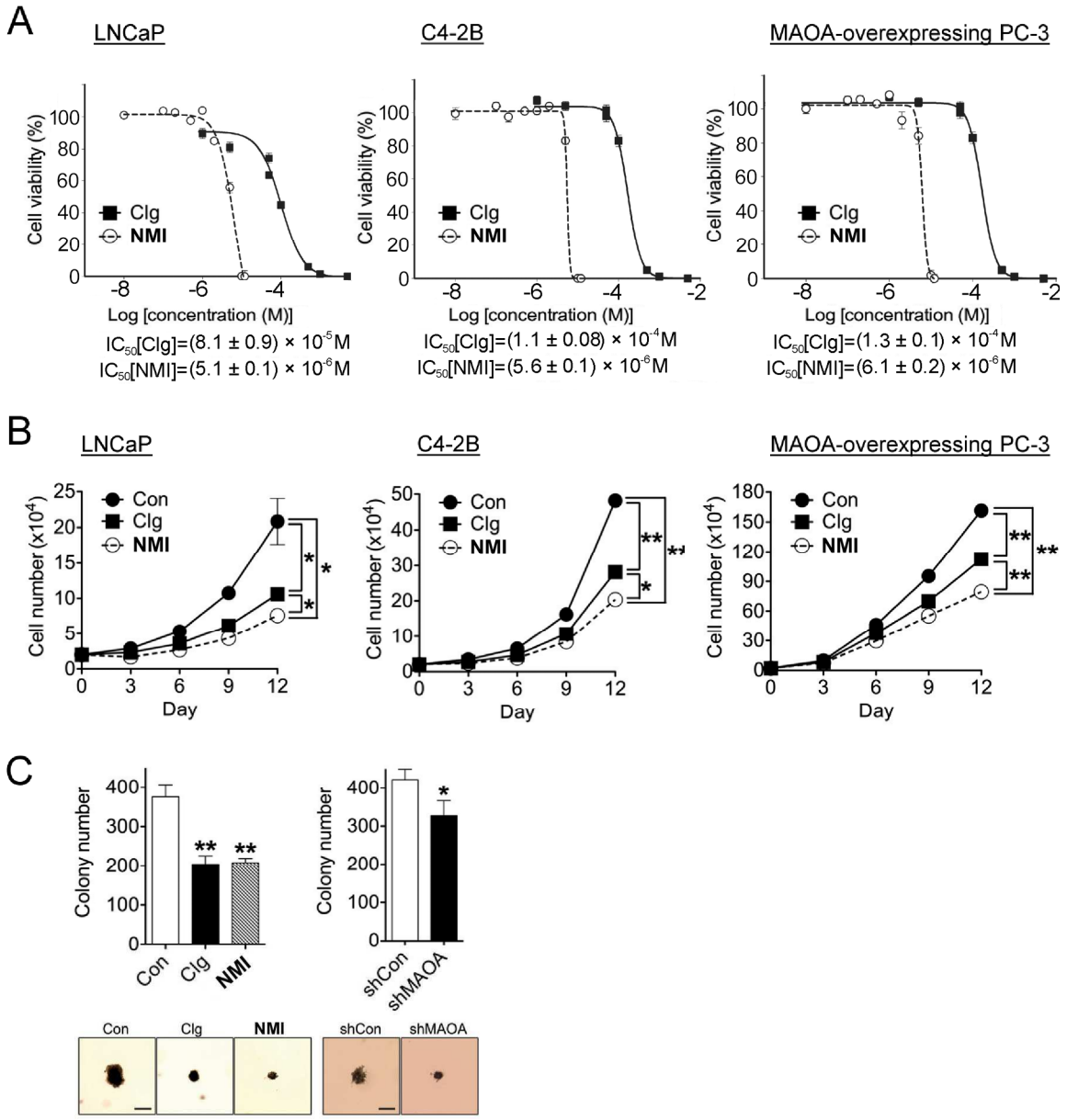

Figure 2. **NMI** inhibits PCa cell proliferation and colony formation.
(A) Effect of Clg and **NMI** on cell viability in LNCaP, C4-2B and MAOA-overexpressing PC-3 cells as measured by an MTS assay. (B) Cell number counting assay with LNCaP, C4-2B and MAOA-overexpressing PC-3 cells treated with Clg or **NMI** (1 μM) for 12 days. Compound-added medium was replenished every 3 days, PBS was used as the vehicle. * $p<0.05$. (C) Colony formation assays in either LNCaP cells treated with Clg or **NMI** (1 μM, left panel) or LNCaP cells targeted by either a scrambled shRNA (shCon) or a MAOA-targeting shRNA (shMAOA). Representative colonies are shown (original magnification, ×100, scale bar: 50 μm). * $p<0.05$, ** $p<0.01$.

NMI (Figure 2C). In a parallel setup, LNCaP cells were targeted by either MAOA-targeting shRNA (shMAOA) or a scrambled shRNA (shCon). Treatment with clorgyline and **NMI** resulted in a reduction of the colony number by as much as 45%, although in this assay the difference between the activities of clorgyline and **NMI** was not statistically significant (left panel). Treatment with MAOA-targeting shRNA reduced colony number by only 25%, as compared to treatment with scrambled shRNA (right panel). Because clorgyline has consistently shown lower efficacy in these experiments, we focused on **NMI** in the subsequent studies.

We tested the ability of **NMI** to inhibit migration of LNCaP and C4-2B cells. After treatment with compounds at 1 μM concentration for 48 hours the LNCaP cells showed statistically significant reduction in migration of 35% for **NMI** (Figure 3A, left panel). A similar result was

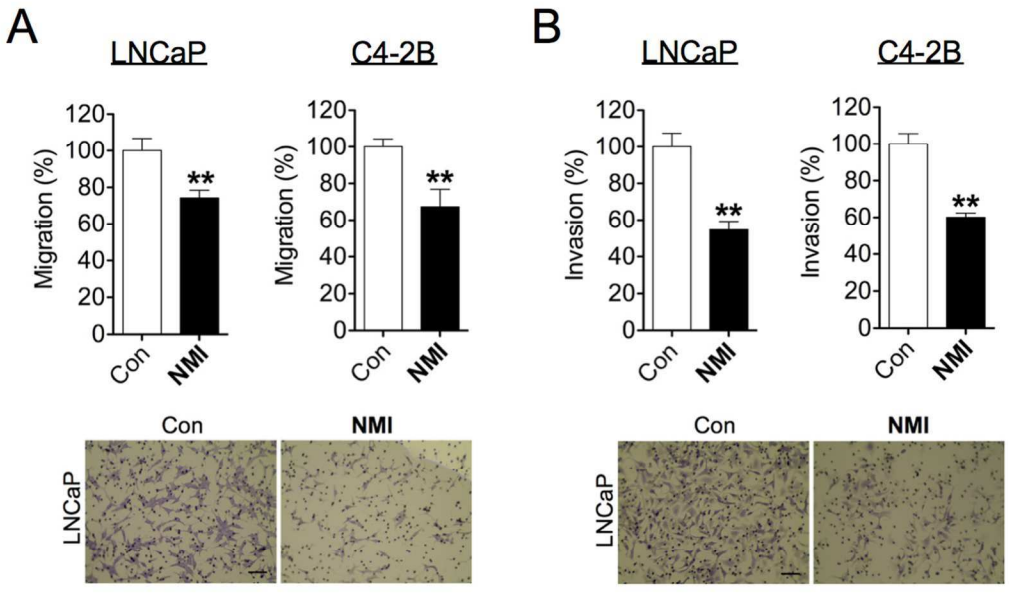

Figure 3. **NMI** reduces the migration and invasion of PCa cells.
(A) Migration assays of LNCaP and C4-2B cells treated with **NMI** (1 μM, 48 hours). ** $p<0.01$. Representative images from LNCaP cells are shown. Original magnification, ×200, scale bar: 200 μm. (B) Invasion assays of LNCaP and C4-2B cells treated with **NMI** (1 μM, 48 hours). ** $p<0.01$. Representative images from LNCaP cells are shown. Original magnification, ×200, scale bar: 200 μm.

observed for C4-2B cells (Figure 3A, right panel). In invasion assays, cells treated with **NMI** also showed 50% reduction in LNCaP and 40-45% in C4-2B cells (Figure 3B).

NMI reduces the rate of growth of PCa xenografts in nude mice.

In order to assess the efficacy of **NMI** *in vivo*, subcutaneous tumor xenograft mouse models were used. After being implanted subcutaneously into male nude mice, C4-2B cells formed tumors in 3-4 weeks. After tumors reached 200 mm^3, mice were randomly assigned into two groups to receive treatments every other day: 1) control and 2) **NMI**. Two routes of administration were used to test the tumor-specific targeting ability of **NMI**: intratumoral and intraperitoneal. Tumors were measured with calipers and tumor volume was calculated every three days during the 21-

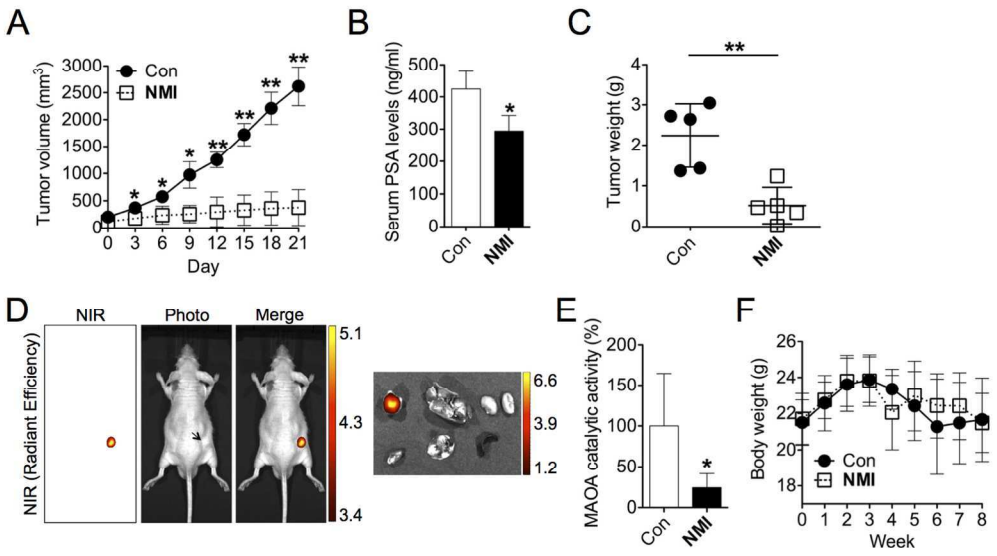

Figure 4. **NMI** inhibits the growth of C4-2B tumor xenografts in mice.
(A) C4-2B cells were subcutaneously injected into male nude mice (n=5 for each group) to establish tumor xenografts. After tumor size reached 200 mm^3, mice were given intratumoral treatments (saline and **NMI**; 750 nmol/mouse) every other day for a 21-day period. Tumor size was determined by calipers and tumor volume calculated as described in Supporting Information. * $p<0.05$, ** $p<0.01$. (B) Serum PSA levels in mice were determined on day 11 since the treatment by ELISA assay. * $p<0.05$. (C) Tumor weight, determined at the time of euthanasia of mice. * $p<0.05$, ** $p<0.01$. (D) *In vivo* and *ex vivo* NIR imaging of mice given **NMI** treatment. Representative images are shown. NIR fluorescence color scales denote $\times 10^9$ and $\times 10^8$ for *in vivo* and *ex vivo* imaging, respectively, in the units of radiant efficiency ([p/sec/cm^2/sr]/[μW/cm^2]). (E) Tumor MAOA catalytic activity was determined at the time of euthanasia. * $p<0.05$. (F) Mice body weight, determined every week since tumor implantation.

day treatment. Serum PSA levels in mice were determined on day 11, the middle of treatment course, and tumor MAOA activity was determined at the end of treatment. Mice body weights were monitored on a weekly basis since the time of inoculation. At the experiment endpoint mice were euthanized, tumors were excised, and tumor weights were determined. **NMI**-treated mice showed significant delays in tumor growth (Figure 4A), reduction in PSA levels (Figure 4B) and decreases in tumor weight as compared to control mice (Figure 4C). NIR imaging of the whole body *in vivo* and individual tumor and normal organs *ex vivo* clearly showed **NMI** localization within the tumor (Figure 4D). Measurements of MAOA activity in tumors showed its significant reduction in **NMI**-treated mice (Figure 4E). All mice in treated and control groups showed similar changes in body weight that did not exceed 18% throughout the entire duration of experiment (Figure 4F), suggesting that this treatment regimen was well tolerated by the animals. We next performed hematoxylin and eosin staining (H&E) and immunohistochemical analysis of protein expression patterns of Ki-67 (a cell proliferation marker), M30 (a cell apoptosis marker) and CD31 (an angiogenesis marker) in tumor specimens from control and treated groups (Figure 5A). H&E staining showed a decrease in the nucleus to cytoplasm ratios in cells from tumors treated by **NMI** as compared to control group, suggesting reduced malignancy in treated tumors.[26] Ki-67 staining of tumor specimens revealed a 30%–35% decrease of Ki-67$^+$ cells in **NMI**-treated tumors (Figure 5B, left panel). We observed 10-12 fold increase of M30$^+$ area (middle panel) and 30-40% decrease in CD31$^+$ area (right panel) in the treated specimens as compared to controls (Figure 5B), suggesting increased apoptosis and reduced angiogenesis occurring in treated tumors.

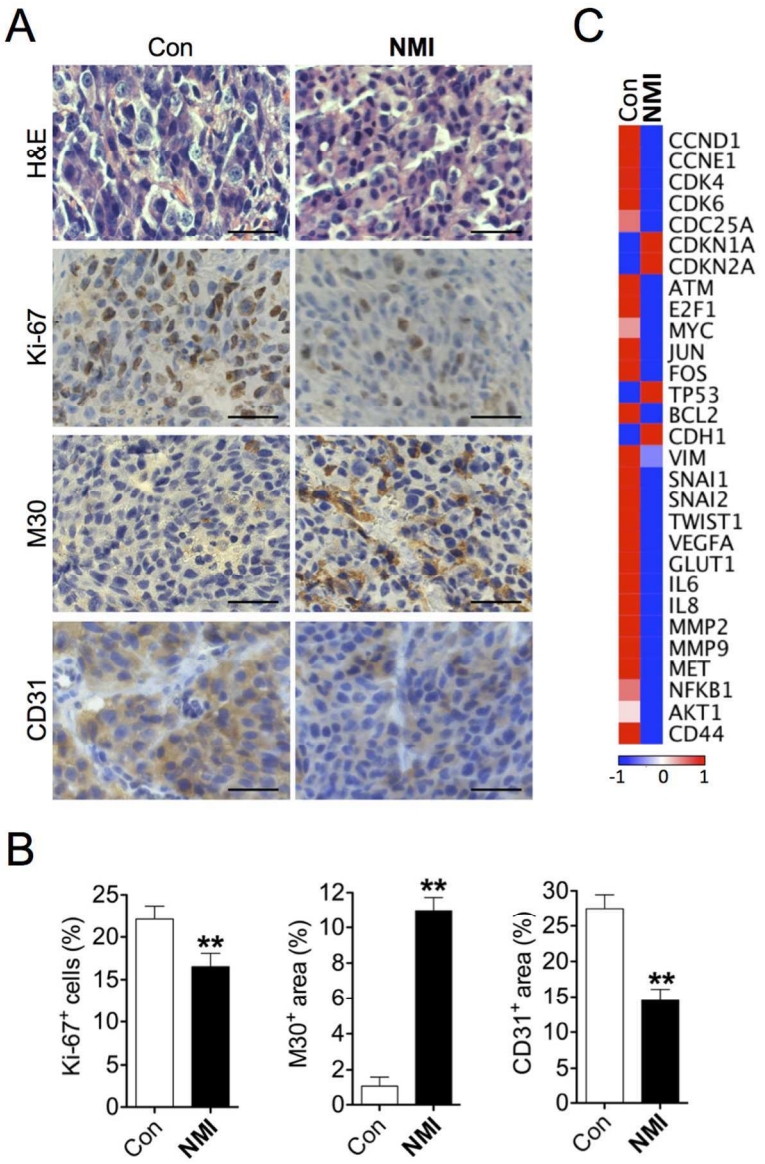

Figure 5. Analysis of tumor specimens obtained from treated and control mice.
(A) H&E and immunohistochemical analysis of Ki-67, M30 and CD31 expression in respective tumor specimens. Representative images are shown. Original magnification, ×400, scale bars: 20 μm. (B) Quantification of percent of Ki-67$^+$, M30$^+$ and CD31$^+$ tumor cells or areas of five distinct images from each group. The data represent mean ± SD. ** p<0.01. (C) Heat map depicting gene expression profiling of tumor samples from each group. Red and blue colors indicate high and low relative expression levels, respectively, with the numbers indicating $\log_2$-transformed ratios.

Gene expression profiling further indicated downregulation in expression of such proto-oncogenes or oncogenes as *FOS*, *JUN NFKB1* and *MYC* and upregulation of *TP53* tumor suppressor gene expression in response to treatment. Cell-cycle regulator genes that activate cell cycle progression, such as *CCND1*, *CCNE1*, *CDK4*, and *CDK6*, were also downregulated, whereas expression of select cell-cycle inhibitors, including *CDKN1A* and *CDKN2A,* has increased in the **NMI**-treated tumors as compared to controls. In contrast, decreased expression of anti-apoptotic *BCL2* gene was revealed in treated tumor samples. In addition, genes involved in MAOA-downstream signaling demonstrated to promote EMT (*VIM*, *SNAI1*, *SNAI2* and *TWIST1*), tumor hypoxia (*VEGFA* and *GLUT1*) and cancer cell migration, invasion and metastasis (*IL6*, *IL8*, *MMP2*, *MMP9* and *MET*)[5] all showed reduced expression by treatment (Figure 5C).

To further evaluate tumor-targeting properties of **NMI**, C4-2B cells were subcutaneously implanted contralaterally into both flanks of male nude mice. After the formation of two tumor xenografts in each mouse, **NMI** was injected intratumorally into one of the lesions. NIR imaging conducted after three injections performed every other day showed localization of the conjugate in both tumors (Figure 6A), which reveals tumor-targeting properties of **NMI**. Remarkably, the intensity of the NIR signals originating from the injected and contralateral tumor was comparable, suggesting rapid redistribution of the injected compound between two tumors. Figure 6B further shows that **NMI** selectively targets two tumors when administered in an intraperitoneal injection. NIR imaging shows no observable NIR signals in other body parts, further confirming the tumor-specific targeting of **NMI** and its systemic circulation.

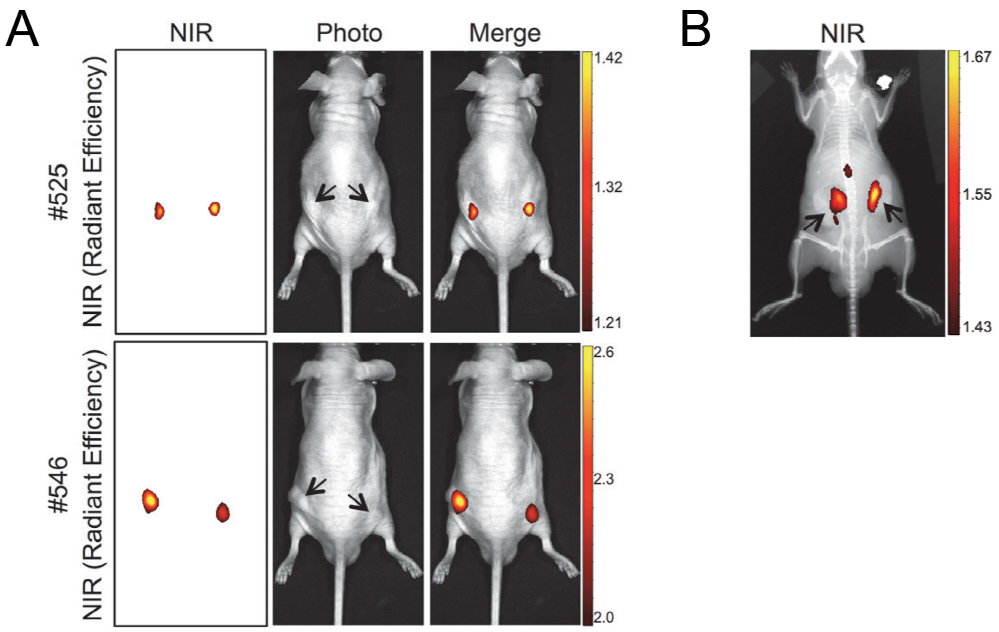

Figure 6. Tumor-targeting properties of **NMI** in mouse xenografts.
(A) C4-2B cells were subcutaneously implanted into both flanks of male nude mice to form tumor xenografts, and the tumor only in one flank (right #525 or left #546) was given intratumoral injection of **NMI** (12 nmol/mouse) every other day for three times followed by NIR imaging. Representative images are shown. (B) Mice bearing C4-2B tumor xenografts as described in (A) were intraperitoneally injected with **NMI** (50 nmol/mouse), and 24 hours later, subjected to NIR imaging. One representative image is shown. Tumors are indicated by the arrows. NIR fluorescence color scales denote $\times 10^9$ and $\times 10^{10}$ for intratumoral and intraperitoneal injections, respectively, in the unit of radiant efficiency ([p/sec/cm^2/sr]/[μW/cm^2]).

Discussion

The search for effective therapies based on pharmacological targeting and inhibition of increased MAOA expression in PCa and potentially other cancers is in its infancy. This study is our first report on the design, synthesis, *in vitro* and *in vivo* evaluation of the therapeutic efficacy of **NMI**, a novel conjugate that targets tumors and reduces MAOA activity in mouse PCa xenograft models. The conjugate consists of the MAOA targeting functionality and a NIR dye. It was synthesized in 8 steps in a scalable procedure from commercially available starting materials to

give hundreds of milligrams of material. The conjugate was shown to target PCa cells, localize in mitochondria and inhibit MAOA activity in the low micromolar IC_{50} range. It has shown efficacy that exceeds clorgyline, a known MAOA inhibitor, in suppressing the growth of three PCa cell lines with high levels of MAOA: LNCaP, C4-2B and MAOA-overexpressing PC-3. It inhibited colony formation for LNCaP cells similarly to that of MAOA-targeting shRNA. **NMI** also inhibited invasion and migration of PCa cells, which is consistent with the demonstrated mechanism that high MAOA activity is associated with aggressive cell behavior and induced EMT. The diminished levels of an epithelial marker E-cadherin and increased expression of a mesenchymal marker vimentin indicates an EMT suppression. By conducting a comparative study using **NMI** and clorgyline, we have shown that the tumor-targeting property of **NMI** makes it a superior pharmacological inhibitor, as compared to clorgyline, in nearly all cases.

Our *in vivo* studies using PCa xenograft mouse models show that **NMI** localizes in the tumors, reduces the rate of tumor growth, and decreases levels of PSA and MAOA catalytic activity in mice engrafted with C4-2B cells. At a final dose of 6 nmol per mouse **NMI** shows significant inhibitory efficacy on tumor xenograft growth. One of the unexpected findings is the discovery that an intratumorally injected compound would redistribute itself into the neighboring tumors, suggesting that its redistribution *in vivo* is facilitated by the rapid circulation in the bloodstream. This is further supported by the observation of tumor-specific targeting made by an intraperitoneal administration.

We previously shown that tumor hypoxia is one of the major factors that mediates an uptake of heptamethine carbocyanine NIR dyes by tumor cells.[22] Hypoxia, through stabilization of HIF1α,

also underlies one of the key MAOA functions in promoting tumor progression and metastasis in PCa.[5] The increased uptake and retention of **NMI** in tumors is likely due to tumor hypoxia through an activated HIF1α/OATPs signaling axis,[22] which is supported by our observation that tumor-targeting effect of **NMI** could be enhanced in PCa expressing high levels of MAOA associated with increased tumor hypoxia. Indeed, the higher accumulation of **NMI** in MAOA-overexpressing PC-3 tumors as compared to control tumor is paralleled by the increase in HIF1α immunostaining in those tumor samples with elevated expression of MAOA (see Supporting Information, Figure S1). These observations suggest that a synergistic strategy based on the use of tumor-targeting MAOA inhibitor such as **NMI** and inhibitors of hypoxia-inducible transcription could result in an improved efficacy and reduced side effects in treating hypoxic, high-grade PCa.

Conclusion

We have demonstrated that tumor-targeting NIR dye - MAOA inhibitor conjugate has the highest efficacy among all the MAOA inhibitors tested in PCa and it may become a novel pharmacological agent for treatment and diagnosis of this type of cancer. Such an agent, after the proper preclinical development, could become an important platform for future generation of anticancer therapeutics. Such conjugate also possesses a diagnostic potential, by differentiating the prostate tumors with high MAOA activity, high hypoxia and elevated malignant potential, from the indolent neoplasms. Its anti-tumor effect, largely derived through MAOA targeting, is making it a valuable addition to the anticancer therapeutic armamentarium.

Experimental Section

General. All reagents and solvents were obtained from commercial sources and were used as received unless otherwise stated. Molecular biology grade salts and buffers were obtained from Sigma-Aldrich. Mitotracker Green and DAPI dyes were obtained from Life Technologies. All reactions involving moisture-sensitive reagents were conducted under argon atmosphere with anhydrous solvents and flame-dried glassware. Hygroscopic liquids were transferred via a syringe and were introduced into reaction vessels through rubber septa. Reaction product solutions were concentrated using a rotary evaporator at 30-150 mm Hg. Column chromatography was performed on silica gel (230-400 mesh) using reagent grade solvents. Analytical thin-layer chromatography (TLC) was performed on glass-backed, pre-coated plates (0.25 mm, silica gel 60, F-254, EM Science). Analytical HPLC were performed on Microsorb-MV C_8 reverse-phase column (250 × 4.6 mm, Varian) using Shimadzu LC-10A VP pump and Shimadzu SPD 10A VP UV-vis variable-wavelength detector. Preparative HPLC purifications were carried out with C_8 reverse phase preparative column (Grace Davison). The flow rate for preparative reverse-phase HPLC was 4 mL/min. In all cases, 5%-95% gradients of acetonitrile in 0.1% aqueous trifluoroacetic acid (TFA) were used as eluents. Water (18 MΩ) was obtained from a Barnstead water purification system, and all buffers were 0.2 μm filtered. Nuclear magnetic resonance (NMR) spectra were collected on instruments in the indicated solvents. The identity and purity of each intermediate and the final product were confirmed by ^{1}H and ^{13}C NMR (Varian Mercury 400 MHz) and mass spectrometry (Agilent 6520 time-of-flight system).

Synthesis of Compounds.

***t*-Butyl (3-bromopropyl)carbamate (2).** To a 100-mL round-bottom flask equipped with a magnetic stirrer was added 3-bromopropylamine hydrobromide (**1**, 1.19 g, 5.44 mmol, 1.0 eq.)

and dichloromethane (30 mL). To the resultant solution was added di-tert-butyl dicarbonate (2.16 g, 9.90 mmol, 1.8 eq.) in dichloromethane (20 mL), followed by triethylamine (0.866 mL, 6.21 mmol, 1.1 eq.). The solution was stirred at room temperature for 75 minutes. The reaction was diluted with dichloromethane (50 mL), and washed twice with sodium bicarbonate (50 mL) and once with brine (50 mL). The organic phase was dried over sodium sulfate, filtered, and the solvent was removed *in vacuo* to yield **2** (1.35 g, 80% yield). ^{1}H NMR (400 MHz, $CDCl_3$) 4.65 (s, 1H), 3.37 (dt, 2H, J_1 = 6.4 Hz, J_2 = 1.2 Hz), 3.21 (dd, 2H, J_1 = 12.4 Hz, J_2 = 6.4 Hz), 1.98 (m, 2H), 1.37 (s, 9H).

***t*-Butyl 3-(2,4-dichlorophenoxy)propylcarbamate (4).** To a 50-mL round-bottom flask equipped with a magnetic stirrer was added 2,4-dichlorophenol (**3**, 452 mg, 2.77 mmol, 1.0 eq.) followed by dimethylformamide (3 mL). To the resultant solution was added sodium hydride portion-wise (111 mg, 2.77 mmol, 1.0 eq.) followed by **4** (661 mg, 2.77 mmol, 1.0 eq.) in DMF (2 mL). The mixture was stirred at 60°C for 3 hours. The reaction was diluted with dichloromethane (50 mL), and washed three times with 10% sodium hydroxide (15 mL), once with HCl (25 mL), and once with brine (50 mL). The organic phase was dried over sodium sulfate, filtered, and the solvent was removed *in vacuo* to yield **4** (431 mg, 48% yield). ^{1}H NMR (400 MHz, $CDCl_3$) 7.36 (d, 1H, J = 2.8 Hz), 7.18 (dd, 1H, J_1 = 8.8 Hz, J_2 = 2.8 Hz), 6.83 (d, 1H, J = 8.4 Hz), 5.16 (s, 1H), 4.07 (t, 2H, J = 5.6 Hz), 3.38 (m, 2H), 2.03 (m, 2H), 1.44 (s, 9H).

***t*-Butyl 3-(2,4-dichlorophenoxy)propyl(prop-2-ynyl)carbamate (6).** To a 20-mL scintillation flask equipped with a magnetic stirrer was added **4** (273 mg, 0.858 mmol, 1.0 eq.) followed by dimethylformamide (3 mL). To the resultant solution was added sodium hydride portion-wise (35 mg, 0.858 mmol, 1.0 eq.) followed by propargyl bromide (**5**, 130 μL, 0.858 mmol, 1.0 eq.). The mixture was stirred at room temperature for 2 hours. The reaction was evaporated and the

residue purified by column chromatography using a gradient of 2%-5%-50% EtOAC in hexanes to provide **6** (75.4 mg, 21% yield). ^{1}H NMR (400 MHz, $CDCl_3$) 7.36 (d, 1H, J = 2.8 Hz), 7.17 (dd, 1H, J_1 = 8.4 Hz, J_2 = 2.4 Hz), 6.83 (d, 1H, J = 8.8 Hz), 4.07 (t, 2H, J = 6.0 Hz), 4.04 (t, 1H, J = 5.6 Hz), 3.56 (t, 2H, J = 6.8 Hz), 2.18 (t, 2H, J = 2.4 Hz), 2.03 (m, 2H), 1.57 (s, 2H), 1.44 (s, 9H).

***N*-(3-(2,4-dichlorophenoxy)propyl)prop-2-yn-1-aminium trifluoroacetate (7).** To a 20-mL scintillation flask equipped with a magnetic stirrer was added **6** (72.6 mg, 0.858 mmol, 1.0 eq.) followed by dichloromethane (4 mL). To the resultant solution was added trifluoroacetic acid (1 mL). The mixture was stirred at room temperature for 8 minutes. The reaction was evaporated and dried *in vacuo* to provide **7** without further purification (75 mg, quantitative yield).

***S*-3-bromopropyl ethanethioate (8).** A 250-mL three-neck round-bottom flask equipped with a thermocouple in a glass sleeve, a magnetic stirrer, a vigreux column with an Argon inlet (middle stem) and a sleeved rubber septum stopper was assembled and dried with a heat gun under flow of argon. Then, approximately 110-120 mL of anhydrous DMF was added via a cannula. Potassium thioacetate (11.68 g, 102.3 mmol) was added by portions into the flask while cooled with ice-cold MeOH bath. The reaction was stirred for 7 hours at about -10°C. Then ice-cold MeOH bath was removed after quenching the reaction by adding 165 mL of water. The reaction mixture was partitioned with 300 mL MTBE and 700 mL water. The water layer was washed by 200 mL MTBE. The MTBE layers were washed sequentially with water, saline and $NaHCO_3$, dried over $MgSO_4$, filtered and evaporated to yield **8** (19.1 g, yield 98.7%). ^{1}H NMR (400 MHz, $CDCl_3$) 3.45 (t, 2H, J = 6.4 Hz), 3.01 (t, 2H, J = 7.2 Hz), 2.35 (s, 3H), 5.16 (s, 1H), 2.13 (m, 2H).

***S*-3-((3-(2,4-dichlorophenoxy)propyl)(prop-2-ynyl)amino)propyl ethanethioate (9).** To a 20-mL scintillation vial equipped with a magnetic stirrer was added **7** (12 mg, 0.032 mmol, 1.0 eq.)

followed by acetonitrile (2.5 mL). To the resultant solution was added potassium carbonate (186 mg, 1.343 mmol, 10.0 eq) followed by **8** (12.6 mg, 5.66 mmol, 17.7 eq). The mixture was stirred at 80°C overnight. The reaction was then filtered, the solvent was removed under reduced pressure and the residue was dried *in vacuo*. The crude material was purified by preparative TLC using 5% ethyl acetate in hexanes as an eluent to give **9.** Yield 4.7mg (39%). ^{1}H NMR (400 MHz, $CDCl_3$) 7.35 (d, 1H, J = 2.4 Hz), 7.16 (dd, 1H, J = 8.4 Hz, J = 2.4 Hz), 7.35 (d, 1H, J = 8.8 Hz), 4.07 (t, 2H, J = 6.0 Hz), 4.04 (t, 1H, J = 5.6 Hz), 3.40 (s, 2H), 2.87 (t, 2H, J = 6.8 Hz), 2.70 (t, 2H, J = 6.4 Hz), 2.56 (t, 2H, J = 6.8 Hz), 2.30 (m, 3H), 2.17 (s, 1H), 1.95 (m, 2H), 1.71 (m, 2H).

3-((3-(2,4-dichlorophenoxy)propyl)(prop-2-ynyl)amino)propane-1-thiol (10). A solution of *S*-3-((3-(2,4-dichlorophenoxy)propyl)(prop-2-ynyl)amino)propyl ethanethioate **9** (1.17 mg, 3.10 μmol) in 200 μL ACN was added into a 20 mL vial equipped with a stir bar, evaporated and then co-evaporated with MeOH 3 times to remove ACN. MeOH/HCl (200 μL) was added into the vial and then the vial was heated on an oil bath at 85°C for 6 hours. The reaction mixture was co-evaporated sequentially with MeOH 3 times and ACN 3 times to give **10** which was used in the next step without further purification.

6-((*Z*)-2-((*E*)-2-(2-chloro-3-((*E*)-2-(1-(6-((3-((3-(2,4-dichlorophenoxy)propyl)(prop-2-yn-1-yl)amino)propyl)thio)-6-oxohexyl)-3,3-dimethyl-3*H*-indol-1-ium-2-yl)vinyl)cyclohex-2-en-1-ylidene)ethylidene)-3,3-dimethylindolin-1-yl)hexanoate (NMI). MHI-148 **11** (170 mg, 242 μmol, 1.10 eq.), dry dichloromethane (10 mL), EDCI hydrochloride (45 mg, 235 μmol, 1.04 eq.), and DMAP (8 mg, 6.5 μmol, 0.03 eq.) were added to a 20-mL round-bottom flask equipped with a stir bar and stirred for 15 minutes. Compound **10**, obtained from the previous step (75 mg, 226 μmol, 1.00 eq.) was added to the mixture as a solution in acetonitrile (2 mL), and the reaction

was stirred at room temperature overnight. The solvent was removed under reduced pressure. The compound was dissolved in 5 mL of dichloromethane and purified on preparative silica gel plates using 7.5% MeOH in dichloromethane as an eluent. Yield 83.2 mg (37%). Alternatively, the reaction mixture aliquot was dissolved in methanol and purified by HPLC using YMC HPLC column, (C_{18} 5-μm column, 50 mm length × 20 mm I.D.) and a 5% - 95% gradient of ACN in 0.1% aqueous trifluoroacetic acid (TFA) over 30 min to yield **NMI** (0.144 mg recovery). ^{1}H NMR (400 MHz, $CDCl_3$): δ 1.49 (m, 2H, γ-C$\underline{H}_2$(COOH)), 1.56 (m, 2H, γ-C$\underline{H}_2$(COSCH$_2$-)), 1.67 (s, 6H,C$\underline{H}_3$), 1.71 (s, 6H,C$\underline{H}_3$), 1.80 (m, 2H, β-C$\underline{H}_2$), 1.82 (m, 2H, β-C$\underline{H}_2$), 1.86 (m, 2H, δ-C$\underline{H}_2$), 1.88 (m, 2H, δ-C$\underline{H}_2$), 1.94 (s, 2H, O-CH$_2$C$\underline{H}_2$CH$_2$N-), 1.97 (s, 2H, S-CH$_2$C$\underline{H}_2$CH$_2$N-), 2.09 (s, 2H, CH$_2$), 2.56-2.57 (m, 4H, α-CH$_2$), 2.68-2.70 (m, 4H, C$\underline{H}_2$NC$\underline{H}_2$), 2.71 (s, 2H, CH$_2$C=), 2.75 (s, 2H, CH$_2$C=), 2.85 (m, 2H, -SC$\underline{H}_2$), 4.04 (t, 1H, $\underline{H}$CΞC-), 4.05 (t, 4H, N-C$\underline{H}_2$), 4.05 (t, 2H, O-C$\underline{H}_2$), 4.07 (t, 2H, CH$_2$CΞ), 6.04 (d, 1H, C$\underline{H}$=CH), 6.32 (d, 1H, C$\underline{H}$=CH), 6.85 (d, 1H, Ar-$\underline{H}$), 7.05 (d, 1H, Ar-$\underline{H}$), 7.17 – 7.42 (m, 9H, Ar-$\underline{H}$), 8.28 (d, 1H, CH=C$\underline{H}$), 8.40 (d, 1H, CH=C$\underline{H}$). HRMS calcd. for $C_{57}H_{69}Cl_3N_3O_4S$ *m/z* 996.4074; observed *m/z* 996.4068. λ_{max} absorption and fluorescence wavelengths in methanol were 780 and 802 nm, respectively.

Cell lines and cell culture conditions. Human PCa LNCaP cell line was obtained from American Type Culture Collection. Human PCa C4-2B cell line was established from LNCaP as described previously.[27] Human PCa MAOA-overexpressing PC-3 cell line was established as described previously.[5] LNCaP and C4-2B cells were grown in RPMI 1640 medium (Life Technologies) and MAOA-overexpressing PC-3 cells were grown in T-medium (Life Technologies), with both media supplemented with 10% fetal bovine serum (FBS) and 1% penicillin/streptomycin.

Laser-scanning confocal microscopy. Cells were plated in glass bottom microscopy dishes (MatTek) at a density of 20,000 cells in 400 µl of medium supplemented with 10% FBS and were allowed to form a monolayer over 20 hours. **NMI** at a concentration of 5 µM in 400 µL of fresh medium containing 10% FBS, MitoTracker Green (1×) and DAPI (1×) were added to the media and the cells were incubated at 37°C and 5% CO_2 for additional 4 hours. Imaging was performed on a Zeiss LSM 510 inverted laser-scanning confocal microscope, equipped with an oil-immersion ×63 objective lens. Excitation wavelengths were set at λ_{max} = 488 nm (DAPI, blue excitation), 514 nm (MitoTracker Green, green-yellow excitation) and 790 nm (**NMI**, red excitation). The data were acquired in a multi-track mode. Images were taken using the pinholes of 130-200 µM in order to capture fluorescence signals on a thin focus plane.

MAOA catalytic activity assay. MAOA catalytic activity was determined in PCa cells and tumor samples treated with clorgyline or **NMI** at different concentrations. One hundred micrograms of total protein (~1×10^6 cells) were incubated with 1 mM ^{14}C-5-hydroxytryptamine (5-HT) in the assay buffer (50 mM sodium phosphate buffer, pH 7.4) at 37^{o}C for 20 minutes, and the reaction was terminated by the addition of 100 µL of 6N HCl. The reaction products were extracted with benzene/ethyl acetate and centrifuged. The organic phase containing the reaction products was extracted, and the radioactivity was determined by liquid scintillation spectroscopy.

Cell proliferation assays. Cells were seeded on 96-well plates in triplicate and treated with vehicle, clorgyline or **NMI** at different concentrations for 96 hours. Cell proliferation was determined by MTS assay (Promega) following the manufacturer's instructions. For cell number

counting assays, cells were seeded on 6-well plates (2×10^4 cells/well) and treated with vehicle, clorgyline (1 μM) or **NMI** (1 μM) for 12 days with compound-added medium replenished every 3 days. Cell numbers from triplicate wells were counted by hemocytometer.

Colony formation assay. Cells were suspended in the culture media containing 0.3% agarose (FMC BioProducts) with vehicle, clorgyline (1 μM) or **NMI** (1 μM), and placed on top of solidified 0.6% agarose in 6-well plates. The developed colonies were counted and recorded under a microscope after 3-week incubation.

Migration and invasion assays. Assays were performed using 6.5 mm transwell (8 μm pore size) coated with either collagen I or Growth Factor Reduced Matrigel (BD Biosciences) for the migration and invasion assays, respectively. Cells were serum-starved overnight before seeding to eliminate the interference of proliferative effect with cell migration or invasion. Cells were seeded inside transwell inserts containing culture medium without serum and with treatment. After 18-24 hours, the cells that translocated to the lower surface of the filters were fixed in 4% formaldehyde. The fixed membranes were stained using crystal violet (1% solution). Assays were quantified by counting of the number of stained nuclei in 5 independent fields in each transwell.

Mouse subcutaneous tumor xenograft studies. Male 4- to 6-week-old athymic nude mice were purchased from Taconic, Inc., housed in the animal research facility at University of Southern California (USC), and fed a normal diet. For xenograft studies, 2×10^6 C4-2B cells were mixed 1:1 with Matrigel (BD Biosciences) and injected subcutaneously into nude mice with each

mouse bearing one tumor on the right flank. After tumors reached a size of 100-200 mm^3, mice were randomly assigned to two groups (saline or **NMI**, n=5 per group). For the treatment group, intratumoral injections of **NMI** (2 μg/tumor, 250 nmol/mouse) were given to mice every other day for first 10 days, then the dose was increased to 6 μg/tumor (750 nmol/mouse). Intratumoral injections of saline were given to control group. Tumor size was measured every 3 days by calipers, and tumor volume was calculated by the formula of length × $width^2$ × 0.52.[28] Tumors were dissected and weighted when mice were euthanized on day 21. Mice body weight was measured on a weekly basis since tumor implantation. All animal studies received prior approval by the USC IACUC and were conducted in compliance with its recommendations.

Analysis of tumor uptake of NMI by NIR fluorescence optical imaging. Mice bearing C4-2B subcutaneous tumors, when tumor size reached 2-6 mm in diameter assessed by palpation, were injected intratumorally (3 consecutive injections every other day) with **NMI** at a dose of 12 nmol/mouse or intraperitoneally (1 injection) at 50 nmol/mouse, respectively. Whole-body NIR fluorescence optical imaging was taken at 24 hour after the last injection using an IVIS Lumina XR imaging system (PerkinElmer) equipped with fluorescence filter sets (excitation/emission, 783/840 nm) as described previously.[29] During imaging, mice were maintained in an anesthetized state.

Immunohistochemistry. Immunohistochemical analysis of tumor xenograft samples was performed using antibodies against Ki-67 (Abcam), M30 (DiaPharma), or CD31 (Santa Cruz) following our published protocol[30] with minor modifications. Briefly, formalin-fixed paraffin-embedded sections (4 μm) were deparaffinized, rehydrated, and subjected to antigen retrieval.

After incubation in Dual Endogenous Enzyme Block solution (Dako) for 10 minutes, the section was treated with primary antibody diluted by different folds with Antibody Diluent solution (Dako) at 4^{o}C overnight. The section was then washed 3 times in PBST (PBS containing 0.2% Tween-20) for 5 minutes per washing. To detect specific staining, the section was treated for 30 minutes with EnVision + Dual Link System-HRP (Dako), which contained HRP-conjugated goat antibodies against mouse or rabbit IgG. The section was washed 3 times for 5 minutes each, and specific stains were developed with 3'3-diaminobenzidine (Dako). Imaging acquisition was performed using a Nikon camera and software. Magnification was ×400 (scale bars ~20 μm). Percent of Ki-67^{+} cells and M30^{+} and CD31^{+} area was analyzed by ImageJ software (NIH).

Statistical analysis. Data are presented as the mean ± SD as indicated in the figure legends. All comparisons were analyzed by unpaired 2-tailed Student's *t*-test. A *p*-value less than 0.05 was considered to be statistically significant.

Acknowledgments. This work was supported by the US Department of Defense Prostate Cancer Research Program grant W81XWH-12-1-0282 (to J.C. Shih, B.Z. Olenyuk and H.E. Zhau), the Daniel Tsai Family Fund (to J.C. Shih), Boyd and Elsie Welin Professorship (to J.C. Shih), NIH/National Cancer Institute grants 5P01CA098912, R01CA122602, Board of Governors Endowed Cancer Chair and Margaret E. Early Medical Research Trust Award (to L.W.K. Chung), and by the University of Southern California (to B.Z. Olenyuk). We thank Bin Qian (Department of Pharmacology and Pharmaceutical Sciences, University of Southern California, Los Angeles, CA), Yi-Ting Chen (Uro-Oncology Research Program, Department of Medicine, Cedars-Sinai Medical Center, Los Angeles, CA) for technical assistance. We also

thank Dr. Ramin Dubey, Dr. Vladimir Neschadimenko, and Ms. Li Zhou (Department of Pharmacology and Pharmaceutical Sciences, University of Southern California, Los Angeles, CA) for help in synthesizing **NMI** and precursors.

Supporting Information Available. Figure S1, detailed description of reverse transcription and quantitative real-time PCR assays and Table S1. This material is available free of charge via the Internet at http://pubs.acs.org/.

References:

(1) Bortolato, M.; Chen, K.; Shih, J. C. *Adv. Drug Deliv. Rev.* **2008**, *60*, 1527.

(2) Shih, J. C.; Chen, K.; Ridd, M. J. *Annu. Rev. Neurosci.* **1999**, *22*, 197.

(3) Josson, S.; Nomura, T.; Lin, J. T.; Huang, W. C.; Wu, D.; Zhau, H. E.; Zayzafoon, M.; Weizmann, M. N.; Gururajan, M.; Chung, L. W. *Cancer Res.* **2011**, *71*, 2600.

(4) Sung, S. Y.; Hsieh, C. L.; Law, A.; Zhau, H. E.; Pathak, S.; Multani, A. S.; Lim, S.; Coleman, I. M.; Wu, L. C.; Figg, W. D.; Dahut, W. L.; Nelson, P.; Lee, J. K.; Amin, M. B.; Lyles, R.; Johnstone, P. A.; Marshall, F. F.; Chung, L. W. *Cancer Res.* **2008**, *68*, 9996.

(5) Wu, J. B.; Shao, C.; Li, X.; Li, Q.; Hu, P.; Shi, C.; Li, Y.; Chen, Y. T.; Yin, F.; Liao, C. P.; Stiles, B. L.; Zhau, H. E.; Shih, J. C.; Chung, L. W. *J. Clin. Invest.* **2014**, *124*, 2891.

(6) Flamand, V.; Zhao, H.; Peehl, D. M. *J Cancer Res Clin Oncol* **2010**, *136*, 1761.

(7) True, L.; Coleman, I.; Hawley, S.; Huang, C. Y.; Gifford, D.; Coleman, R.; Beer, T. M.; Gelmann, E.; Datta, M.; Mostaghel, E.; Knudsen, B.; Lange, P.; Vessella, R.; Lin, D.; Hood, L.; Nelson, P. S. *Proc. Natl. Acad. Sci. USA* **2006**, *103*, 10991.

(8) Zhao, H.; Flamand, V.; Peehl, D. M. *BMC Med. Genomics* **2009**, *2*, 55.

(9) Jemal, A.; Siegel, R.; Xu, J.; Ward, E. *CA Cancer J. Clin.* **2010**, *60*, 277.

(10) da Silva, F. C. *Curr. Opin. Urol.* **2011**, *21*, 248.

(11) Wilkins, A.; Parker, C. *Nat. Rev. Clin. Oncol.* **2010**, *7*, 583.

(12) Kapoor, D. A.; Zimberg, S. H.; Ohrin, L. M.; Underwood, W., 3rd; Olsson, C. A. *J. Urol.* **2011**, *186*, 860.

(13) Wang, G. L.; Jiang, B. H.; Rue, E. A.; Semenza, G. L. *Proc. Natl. Acad. Sci. USA* **1995**, *92*, 5510.

(14) Chandel, N. S.; Maltepe, E.; Goldwasser, E.; Mathieu, C. E.; Simon, M. C.; Schumacker, P. T. *Proc. Natl. Acad. Sci. USA* **1998**, *95*, 11715.

(15) Kaelin, W. G., Jr.; Ratcliffe, P. J. *Mol. Cell* **2008**, *30*, 393.

(16) Gerald, D.; Berra, E.; Frapart, Y. M.; Chan, D. A.; Giaccia, A. J.; Mansuy, D.; Pouyssegur, J.; Yaniv, M.; Mechta-Grigoriou, F. *Cell* **2004**, *118*, 781.

(17) Lu, X.; Kang, Y. *Clin. Cancer Res.* **2010**, *16*, 5928.

(18) De Colibus, L.; Li, M.; Binda, C.; Lustig, A.; Edmondson, D. E.; Mattevi, A. *Proc. Natl. Acad. Sci. USA* **2005**, *102*, 12684.

(19) Luo, S.; Zhang, E.; Su, Y.; Cheng, T.; Shi, C. *Biomaterials* **2011**, *32*, 7127.

(20) Tan, X.; Luo, S.; Wang, D.; Su, Y.; Cheng, T.; Shi, C. *Biomaterials* **2012**, *33*, 2230.

(21) Luo, S.; Tan, X.; Qi, Q.; Guo, Q.; Ran, X.; Zhang, L.; Zhang, E.; Liang, Y.; Weng, L.; Zheng, H.; Cheng, T.; Su, Y.; Shi, C. *Biomaterials* **2013**, *34*, 2244.

(22) Wu, J. B.; Shao, C.; Li, X.; Shi, C.; Li, Q.; Hu, P.; Chen, Y.-T.; Dou, X.; Sahu, D.; Li, W.; Harada, H.; Zhang, Y.; Wang, R.; Zhau, H. E.; Chung, L. W. K. *Biomaterials* **2014**, *35*, 8175.

(23) Yang, X.; Shi, C.; Tong, R.; Qian, W.; Zhau, H. E.; Wang, R.; Zhu, G.; Cheng, J.; Yang, V. W.; Cheng, T.; Henary, M.; Strekowski, L.; Chung, L. W. *Clin. Cancer Res.* **2010**, *16*, 2833.

(24) Gordon, R. R.; Wu, M. C.; Huang, C. Y.; Harris, W. P.; Sim, H. G.; Lucas, J. M.; Coleman, I.; Higano, C. S.; Gulati, R.; True, L. D.; Vessella, R.; Lange, P. H.; Garzotto, M.; Beer, T. M.; Nelson, P. S. *PLoS One* **2014**, *9*, e104271.

(25) Murphy, D. L.; Lipper, S.; Slater, S.; Shiling, D. *Psychopharmacology* **1979**, *62*, 129.

(26) Foraker, A. G. *Cancer* **1954**, *7*, 884.

(27) Thalmann, G. N.; Anezinis, P. E.; Chang, S. M.; Zhau, H. E.; Kim, E. E.; Hopwood, V. L.; Pathak, S.; von Eschenbach, A. C.; Chung, L. W. *Cancer Res.* **1994**, *54*, 2577.

(28) Tomayko, M. M.; Reynolds, C. P. *Cancer Chemother. Pharmacol.* **1989**, *24*, 148.

(29) Yang, X.; Shi, C.; Tong, R.; Qian, W.; Zhau, H. E.; Wang, R.; Zhu, G.; Cheng, J.; Yang, V. W.; Cheng, T.; Henary, M.; Strekowski, L.; Chung, L. W. *Clin. Cancer. Res.* **2010**, *16*, 2833.

(30) Zhau, H. E.; Odero-Marah, V.; Lue, H. W.; Nomura, T.; Wang, R.; Chu, G.; Liu, Z. R.; Zhou, B. P.; Huang, W. C.; Chung, L. W. *Clin. Exp. Metastasis* **2008**, *25*, 601.

TOC Graphic

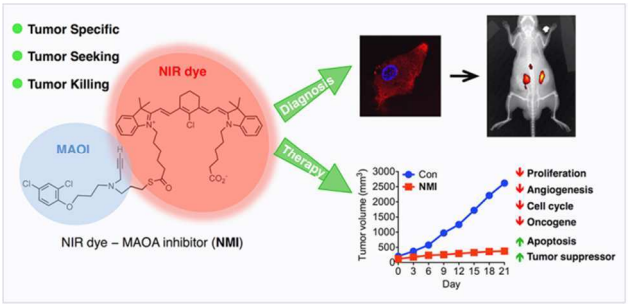
Tumor Specific
Tumor Seeking
Tumor Killing
NIR dye
MAOI
NIR dye – MAOA inhibitor (NMI)
Diagnosis
Therapy
Con
NMI
Tumor volume (mm³)
Day
Proliferation
Angiogenesis
Cell cycle
Oncogene
Apoptosis
Tumor suppressor

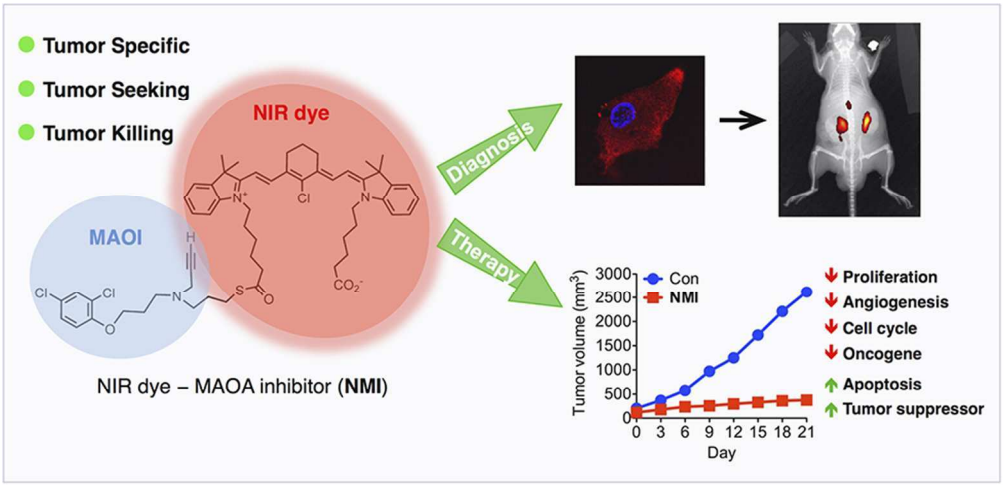

82x39mm (300 x 300 DPI)